Proceedings of the 2006 IEEE International Conference on Robotics and Automation
Orlando, Florida - May 2006

# Designing Open-Loop Plans for Planar Micro-Manipulation

David J. Cappelleri*, Jonathan Fink*, Barry Mukundakrishnan*, Vijay Kumar*, and J. C. Trinkle†

*GRASP Lab
University of Pennsylvania
Philadelphia, PA 19104–6389
Email: {dcappell, jonfink, bharathm, kumar}@grasp.upenn.edu

†Dept. of Computer Science
Rensselear Polytechnic Institute
Troy, NY 12180–3590
Email: trink@cs.rpi.edu

***Abstract*— This paper describes a test-bed for planar micro manipulation tasks and a framework for planning based on quasi-static models of mechanical systems with frictional contacts. We show how planar peg-in-the-hole assembly tasks can be designed using randomized motion planning techniques with Mason's models for quasi-static manipulation. Finally, we present simulation and experimental results in support of our methodology.**

## I. Introduction

While mass production techniques derived from hard automation are routinely applied to micro and meso scale parts, we are not able to achieve micro and meso scale assembly in a semi-structured environment with uncertainties. Indeed, reliably manipulating parts at this scale remains challenging. There are many reasons for this. We lack good models of mechanics of contact interactions at this scale. It is difficult to measure forces at the micro-netwon level reliably using off-the-shelf force sensors and force-feedback control schemes have not proved successful. Finally, it is even more difficult to grasp and manipulate parts at the micro and meso level than it is at the macro level.

A natural question, one that has been asked before [1]–[3], is if simple open loop plans that do not require precise feedback in real-time, can be designed to accomplish such tasks. In this paper we explore such open loop plans for micro-assembly [1] tasks. We limit ourselves to manipulation in a plane and to pushing operations that involve pushing planar parts with a simple probe. The open-loop manipulation task that we are interested in is complicated due to the fact that the manipulated object is subject to an unknown and hard-to-model distribution of contact forces between the support surface and the object as well as unknown frictional contact forces between the probe (pusher) and the object and between the object and its environment. This is further complicated by the fact that contacts are intermittent. Clearly analytical solutions to the forward dynamics problem are impossible except in the simplest of cases, so simulation-based solutions are the only option.

The derivation of the fundamental mechanics of pushing operations and sliding objects have been extensively studied by [4]–[6]. There is also extensive work addressing the analysis and simulation of mechanical systems with frictional contacts. In particular, semi-implicit and instantaneous-time models for predicting motion and contact forces for quasi-static multi-rigid-body systems have recently been developed [7], [8].

Pushing operations and the instantaneous motions of a sliding object during multiple contact pushing are examined and the manipulation primitive of stable rotational pushing is defined in [9]. The problem of planning pushing paths using stable pushes is discussed in [10].

Open-loop motion strategies, without the use of sensors, can be used to eliminate uncertainty and to orient polygonal parts [1], [2], [11]. In [1], planar parts are considered polygons if their convex hull is a polygon. Given a list of $n$ vertices describing the polygonal part with an unknown initial orientation, the shortest sequence of mechanical parallel-jaw gripper actions that will guarantee the orientation of the part up to symmetry is determined. In [2], a randomly oriented planar object is dropped into a tray. Then, using the mechanics of sliding, an automatic planner is created. The planner finds a sequence of tilting operations to leave the object's orientation completely determined. In [11], the authors study the problem of posing a planar part given initial and goal poses. Specifically, they prove that a multiple push strategy always exists (in the absence of obstacles) and they develop a complete, polynomial-time algorithm to design one possible plan.

Sensorless orientation of parts is applied to micro-scale parts in [3]. At the micro scale, sticking effects due to Van der Walls forces and static electricity make the manipulator motions and part release more complicated [12], [13]. Micro-manipulators also have limited degrees of freedom when compared to manipulators at the macro-scale. These problems are addressed in [3] with a parallel-jaw gripper and squeeze and roll primitives to orient a randomly oriented polygonal part up to $180^\circ$ symmetry.

On the other hand, the literature addressing micro-

[1] Although the characteristic lengths of parts of interest are around 1 mm (meso-scale and not micro-scale), we still use the term micro-scale to distinguish us from the macro-scale world in which inertial and gravitational forces generally dominate.

0-7803-9505-0/06/$20.00 ©2006 IEEE

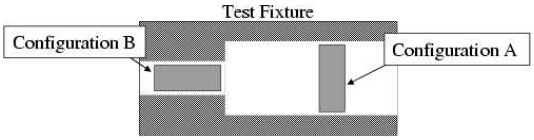


Fig. 1. Peg-in-the-Hole Problem: Move peg from configuration A to configuration B

manipulation with real-time sensor feedback is more limited. The primary reason for this is that obtaining accurate sensor data is a difficult problem at this scale. Sensors cannot easily be affixed to tiny precision instruments without compromising their functionality [13]. The use of high resolution optical systems with controllable parameters for micro-assembly tasks are examined by [14]. Specifically, depth-from-defocus and visual servoing strategies are presented. Even with this sensor data, calibration and vision-based control at this scale can present technical difficulties. Without accurate sensor data, it is hard to to develop models, and therefore controllers, for micro manipulation.

Our work in this paper is in the spirit of our own earlier work [15], where the designer chooses the system parameters relating to geometric, material, and dynamic properties to optimize the performance of the design of an assembly/feeding device. We consider the canonical assembly problem as shown in Figure 1. It consists of moving a peg from configuration A to configuration B by means of a series of pushing operations. The peg-in-the-hole insertion task at the micro scale involves small parts moving at slow speeds (and accelerations) so that the inertial forces are negligible. Indeed surface friction forces are the dominant forces at this scale.

Our goal, in this paper, is to use simulation and motion planning tools to design open loop manipulation plans that rely only on an estimate of initial position and orientation. We use Mason's quasi-static models for manipulation of planar parts with surface friction [4]. The method for 3-D simulation presented in [8] is adapted to solve the "2.5-dimensional" problem with surface friction. An application of the Rapidly Exploring Random Tree (RRT) algorithm [16] with modifications for dynamic systems described in [17] is used to solve the peg-in-hole insertion task.

## II. Quasi-static Simulation and Planning

Since the inertial forces are negligible compared to frictional forces in our problem, the problem of solving for the motion of the peg is quasi-static in nature. This quasi-static problem together with the frictional constraints and the rigid body constraints can be posed as a complementarity problem [18], [19] and subsequently solved to determine the overall motion of the system at every time-step. Simulation based randomized planning algorithms are then used to design manipulation plans for the peg insertion problem.

### A. 2.5D Complementarity Formulation

The problem of a planar polygonal part sliding with surface friction and quasi-static constraints can be formulated in 3-dimensions as a mixed linear complementarity problem (MLCP) as shown in [8]. For a multi-body system with $n_q$ degrees of freedom, the quasi-static equations of motion and time-stepping are:

$$0 = W_n \lambda_n^{l+1} + W_f \lambda_f^{l+1} + F_{ext} \tag{1}$$

$$q^{l+1} - q^l = hG(q)\nu^{l+1} \tag{2}$$

where $q^l \in \mathcal{R}^{n_q}$ is the generalized configuration vector, $\nu^{l+1} \in \mathcal{R}^{n_\nu}$ is the generalized velocity vector, $G(q) \in \mathcal{R}^{n_q \times n_\nu}$ is the Jacobian matrix , $W_n \in \mathcal{R}^{n_\nu \times (n_c+n_s)}$ contains the normal wrenches for each of the $n_c + n_s$ pushing ($n_c$) and support ($n_s$) contacts with normal constraint forces $\lambda_n \in \mathcal{R}^{(n_c+n_s)}$. $W_f \in \mathcal{R}^{n_\nu \times (2n_c+n_d n_s)}$ contains the frictional wrenches (with the friction cone linearized into $n_d$ directions for each contact) with frictional forces $\lambda_f \in \mathcal{R}^{2n_c+n_d n_s}$, and $F_{ext}$ represents the external forces. The rigid body non-penetration constraint and linearized Coulomb friction law result in a set of complementarity conditions.

The uncertainty in surface pressure distribution between the support surface and the peg can be parameterized by arbitrary three-point support distributions between the support surface and the polygonal object being pushed in the plane as shown in [4]. Assuming a fixed center of mass (COM) of the polygonal body, the normal support forces can be determined uniquely for any three-point planar support distribution.

By partitioning the mixed LCP formulation in [8], we are able to take advantage of these known normal forces for the support points and the assumption that our bodies are constrained to the plane to reduce the dimension of the MLCP that must be solved. The partitioned MLCP is shown below, with the subscript *nk* indicating known quantities relating to the normal force at support points.

$$\begin{pmatrix} 0 \\ \rho_n^{l+1} \\ \rho_{nk}^{l+1} \\ \rho_f^{l+1} \\ s^{l+1} \end{pmatrix} = B \begin{pmatrix} q^{l+1} \\ \lambda_n^{l+1} \\ \lambda_{nk}^{l+1} \\ \lambda_f^{l+1} \\ \sigma^{l+1} \end{pmatrix} + b \tag{3}$$

$$0 \leq \begin{pmatrix} \rho_n^{l+1} \\ \rho_{nk}^{l+1} \\ \rho_f^{l+1} \\ s^{l+1} \end{pmatrix} \perp \begin{pmatrix} \lambda_n^{l+1} \\ \lambda_{nk}^{l+1} \\ \lambda_f^{l+1} \\ \sigma^{l+1} \end{pmatrix} \geq 0 \tag{4}$$

where

$$B = \begin{pmatrix} 0 & W_n & W_{nk} & W_f & 0 \\ {W_n}^T & 0 & 0 & 0 & 0 \\ {W_{nk}}^T & 0 & 0 & 0 & 0 \\ {W_f}^T & 0 & 0 & 0 & E \\ 0 & U & U_k & -E^T & 0 \end{pmatrix} \tag{5}$$

$$b = \begin{pmatrix} F_{ext} \\ \psi_n^l + h\frac{\partial \psi_n^l}{\partial t} - W_n^T q^l \\ \psi_{nk}^l + h\frac{\partial \psi_{nk}^l}{\partial t} - W_{nk}^T q^l \\ h\frac{\partial \psi_f^l}{\partial t} - W_f^T q^l \\ 0 \end{pmatrix} \tag{6}$$

and $W_n^k \in \mathcal{R}^{n_\nu \times n_s}$ corresponds to the normal support forces $\lambda_n^k \in \mathcal{R}^{n_s}$. The friction coefficient matrix $U$ is partitioned into $U^k \in \mathcal{R}^{n_s \times n_s}$ for surface contacts and $U \in \mathcal{R}^{n_c \times n_c}$ denotes the friction coefficient matrix at the pushing supports. Notice that the $G^T$ matrices have been dropped here as they are identity matrices in our problem. $\psi_n$ and $\lambda_n$ are the vectors of gap functions and multipliers associated with the separations in the plane, while $\psi_{nk}$ and $\lambda_{nk}$ are similar quantities for contact forces perpendicular to the plane.

For parts fixed in the plane, the support point gaps $\psi_{nk}^l$ and their time derivatives $\frac{\partial \psi_{nk}^l}{\partial t}$ are both zero. Since the contact support forces are known, we can remove the constraints necessary to solve for these values (the third row of Eq 3). Known support normal forces $\lambda_{nk}$ and $U_k \lambda_{nk}$ are moved into the $b$ vector. The reduced system is:

$$\begin{pmatrix} 0 \\ \rho_n^{l+1} \\ \rho_f^{l+1} \\ s^{l+1} \end{pmatrix} = B \begin{pmatrix} q^{l+1} \\ \lambda_n^{l+1} \\ \lambda_f^{l+1} \\ \sigma^{l+1} \end{pmatrix} + b \tag{7}$$

$$0 \leq \begin{pmatrix} \rho_n^{l+1} \\ \rho_f^{l+1} \\ s^{l+1} \end{pmatrix} \perp \begin{pmatrix} \lambda_n^{l+1} \\ \lambda_f^{l+1} \\ \sigma^{l+1} \end{pmatrix} \geq 0 \tag{8}$$

where

$$B = \begin{pmatrix} 0 & W_n & W_f & 0 \\ {W_n}^T & 0 & 0 & 0 \\ {W_f}^T & 0 & 0 & E \\ 0 & \left[\begin{smallmatrix} U \\ 0 \end{smallmatrix}\right] & -E^T & 0 \end{pmatrix}, b = \begin{pmatrix} 0 \\ \psi_n^l + h\frac{\partial \psi_n^l}{\partial t} - W_n^T q^l \\ -W_f^T q^l \\ \left[\begin{smallmatrix} 0 \\ U_k \lambda_{nk} \end{smallmatrix}\right] \end{pmatrix} \tag{9}$$

Note that control input(s) to the system appear in the time-varying function $\psi_n(t)$ and is derivative $\frac{\partial \psi_n}{\partial t}$.

### B. Randomized Planning

We developed a sampling based motion planning algorithm inspired by the RRT algorithm [16] with modifications for dynamic systems described in [17]. Instead of searching for continuous input trajectories $u(q,t)$, we parameterize the input by a $r$-dimensional vector $\underline{u}$ using piecewise-constant functions with compact support.

## III. Peg-in-the-Hole Task

### A. Problem Formulation

The goal is to determine a sequence of manipulator steps that will successfully accomplish the peg-in-hole task as shown in Figure 1. To model this system, suppose the rectangular peg has three support points at positions $r_1$, $r_2$, $r_3$ from the COM. The peg is oriented at $\theta$ degrees from horizontal and the manipulator (probe) is pushing at a point $p$.

The configuration of the peg $q \in \mathcal{R}^3$ is $[x, \ y, \ \theta]^T$. Following the formulation in the previous section, $n_c = 1$, $n_s = 3$. In our implementation, we have chosen to use $n_d = 8$ as we have found an agreeable tradeoff between accuracy and performance with this linearization. $U$ is a $1 \times 1$ matrix with value $\mu$. $U_k$ is $3 \times 3$ with the surface friction coefficient in diagonal entries. $\lambda_{nk}$ is a column vector with the normal forces calculated based on support point locations.

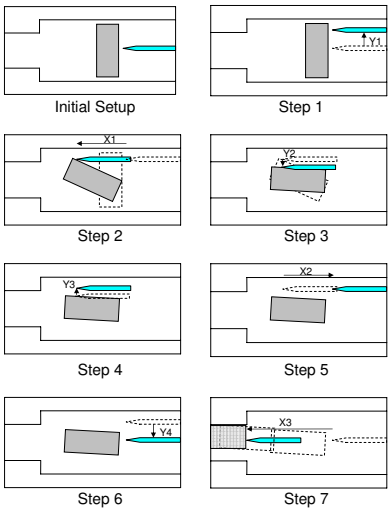


Fig. 2. Open-Loop motion plan for assembly

The $E$ matrix is a binary block-diagonal matrix, each column of which has a non-zero entry corresponding to the directions along which friction acts. The first column corresponds to the directions along which friction between the probe and peg can act. The other three columns correspond to the support point friction directions.

In Equation 9, the gap until peg collision with the fixture or probe is given by $\psi_n^l$ with time derivatives $\frac{\partial \psi_n^l}{\partial t}$ and $\frac{\partial \psi_f^l}{\partial t}$ giving the normal velocity and sliding velocity of a contact. The particular $\psi_n^l$ for the probe contact will be zero and the associated $\frac{\partial \psi_n^l}{\partial t}$ will be the probe velocity.

### B. Manipulation Plan

For a given configuration of the peg, the control inputs explored by the motion planner are determined by calculating and discretizing the peg edges that can be pushed by the probe. Further, we required one of the two components of the motion of the probe to be zero. In other words, for simplicity, we restricted ourselves to motions along the $x$ or $y$ axes.

When a peg state near the specified goal is reached, the algorithm computes the series of manipulator movements to apply each necessary control input. The manipulation plan is completely represented as a vector $\underline{u}$ where each element corresponds to a probe movement command. Each element $\Delta u_i$ is related to the quasi-static time-stepping model by: $\frac{\partial \psi_n^l}{\partial t} = \frac{\Delta u_i}{T_i}$ where $T_i$ is the duration of the push and determined by the probe velocity. A probe movement command will be $\Delta u_i$ = ($\Delta x$,0) or (0,$\Delta y$) corresponding to a probe movement of X or Y along the x-axis or y-axis, respectively (see Figure 2).

Figure 2 shows a schematic of an intuitive open-loop manipulation plan for accomplishing the task. The motion planning algorithm results in a plan similar in nature, but with more steps, not pictured here.

This type of formulation and planning is not restricted to only rectangular parts. Rather, it can be generalized to work

for different shaped parts and other planar examples.

## IV. Micro-manipulation Test-Bed

### A. Experimental Setup

The experimental setup consists of an inverted optical microscope (Nikon Eclipse TEU2000-U), 4-axis micro-manipulator (Siskiyou Design Instruments MX7600R), controller (Siskiyou Design Instruments MC2000), 25 $\mu$m tip tungsten probe (needle), CCD camera (Sony XC-77), and control computer (Figure 3). There is a 4X objective attached to the microscope, producing a field of view (FOV) of 3.37 mm x 2.52 mm. The CCD camera records the images in the FOV and sends them to the control computer at 30 Hz. The micromanipulator and controller allows incremental motion as small as 0.1 $\mu$m in 4 axes - X,Y,Z, and tool axes, respectively.

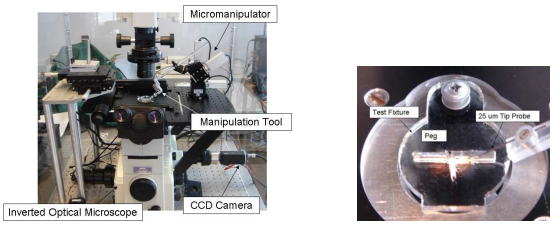


(a) System overview (b) Close-up

Fig. 3. Experimental setup

The test fixture and pegs were made out of mirrored acrylic, machined using the ULS 660 Laser Cutter. The fixture is 3.175 mm (1/8") thick and has 2 channels of different widths machined in it. The larger channel is 2015 $\mu$m wide, while the smaller channel is 1090 $\mu$m wide. A thin plastic sheet is fastened to the bottom of the fixture to allow for a transparent surface where the peg sliding can reside. This transparent quality is needed since the light source for the inverted microscope is projected up from underneath the fixture. Various size pegs were used in testing and they have typical dimensions of 1615 $\mu$m x 985 $\mu$m. The pegs are half the thickness of the acrylic fixture. An image capture of the fixture, peg, and manipulation probe under the microscope is shown in Figure 4. Due to the small size and mass of the peg, it is apparent that the gravity or inertial forces do not dominate during pushing operations [13]. Coupling this with the slow moving probe (140 $\mu$m/sec), one can see that the inertial forces of the peg are much less than the contact force so frictional forces are needed to maintain equilibrium. Therefore, it is reasonable to assume the frictional forces dominate to apply quasi-static modeling of these experiments.

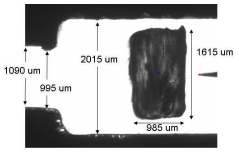


Fig. 4. Fixture and peg as seen in microscope FOV

Image processing techniques are applied to the images (640x480 pixels) from the microscope to track the position of the peg and probe during each experiment. Background subtraction is used to remove the image of the fixture from the original image. Thresholding is used to clean-up the image, producing an image where the peg and probe pixels are black while everything else is white. The image is segregated further by exploiting the geometry of the probe to remove it from the filtered image. During this process, the coordinates of the tip of the probe are identified. An ellipsoid is fitted to the resulting blob image yielding the centroid and orientation of the peg in each image frame.

## V. Experimental Results

### A. System Identification

Our simulation of the peg depends on several critical system parameters including the location of the support points and friction coefficients. Though our goal is to design open-loop plans that will be robust to these uncertainties, some nominal values still must be identified. To solve this system identification problem, we captured data for several experimental trials of the probe pushing the peg. We then found the support point distributions and friction coefficients that produced simulations to best match the experimental results.

To determine the coefficient of friction between the probe and peg we performed a series of simulations sweeping through the one-dimensional space of friction coefficients $\mu$ (from 0 to 1.0). For each experimental trial we performed 100-150 simulations with randomly selected support points that are constrained to lie within the peg dimensions and span the center of mass. Mean squared error for position (X,Y) and orientation $(\theta)$ was computed across the random support distributions for each trial as shown in Table I.

TABLE I
MSE for Unconstrained Motion Test

| Exp. # | # of Sim Trials | $X$,$Y$ MSE | $\Theta$ MSE |
|---|---|---|---|
| 1 | 121 | 2.9113 | 0.0694 |
| 2 | 150 | 2.4458 | 0.0691 |
| 3 | 150 | 5.4378 | 0.0607 |
| 4 | 115 | 2.9310 | 0.0724 |
| 5 | 123 | 3.1908 | 0.0569 |
| 6 | 111 | 7.7284 | 0.0788 |

For the support point configuration that produced the smallest error within a given experimental trial, we ran simulations against the other experimental trials to get a measure of the quality of that support point choice. We found that even though a set of support points was a good fit for a given experimental trial it is not necessarily the best fit to simulate all pushing operations. This serves to emphasize uncertainty in the system and how robust a plan must be to have a high success rate.

Figure 5 shows both the best and worst case trials with the chosen support distribution and our choice of $\mu = 0.8$.

### B. Planning Algorithms Experimental Results

When using an RRT algorithm for dynamic systems, there is always a tradeoff between the coarseness of the discretization

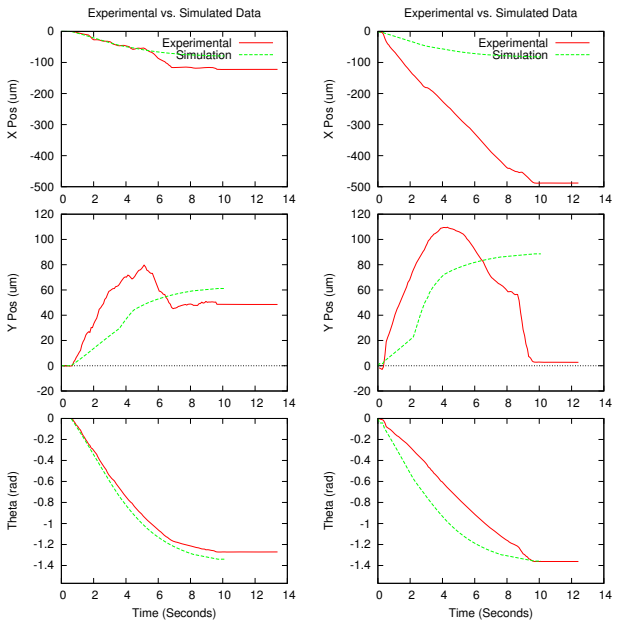


(a) Best Case (b) Worst Case

Fig. 5. Comparison of best and worst trials for matching simulation to experiment with a given choice of support point locations

and the number of iterations necessary to find a goal. For our problem, we found that discretizing the reachable peg surface into 100 pushing locations led to solutions in as few as 12 iterations of the RRT algorithm. However, since the number of control inputs to test at each iteration is large and the LCP based method of simulation can be computationally expensive, the algorithm took on the order of 10 - 20 minutes (on a 1.8GHz PC) to find a solution. Typical solutions include about 7-10 pushing operations which is comparable to our initial, intuitive, solution to the problem. We found that while RRT produced manipulation plans were feasible when used in experimentation and sometimes succeeded, the plans are not robust to error in the support friction modeling or the initial positioning of the peg.

On the other hand, manipulation plans designed with user intuition could be parameterized and tuned using simulation to increase the robustness of the operation to both modeling and positioning error. Table II shows a plan designed with this methodology. Note, the origin for the coordinate frame is the top left corner of the fixture in the image.

Several trials of the intuitive plan with the parameters determined from the simulations were executed on the micro-manipulation test-bed. In the trials, the starting position for the peg varied from the nominal starting position by at most 26 $\mu$m, 74 $\mu$m, and 3° in the x, y, and $\theta$ coordinates. The maximum differences between the peg starting and nominal positions were 11$\mu$m and 21$\mu$m in x and y, respectively. All of the trials resulted in successful placement of the peg in the hole. A plot of the peg and probe tip trajectories for a trial is shown in Figure 6. The starting and ending configuration of

TABLE II

MANIPULATION PLAN PARAMETERS FROM SIMULATOR

| **Peg Start Pos. (X,Y,$\theta$)** | (2.33 mm, 1.21 mm, 89°) |
|---|---|
| **Tip Start Pos. (X,Y)** | (3.05 mm, 1.24 mm) |
| $\Delta u_1$ | $(0, -600)\mu$m |
| $\Delta u_2$ | $(-1500, 0)\mu$m |
| $\Delta u_3$ | $(0, 50)\mu$m |
| $\Delta u_4$ | $(0, -50)\mu$m |
| $\Delta u_5$ | $(1550, 0)\mu$m |
| $\Delta u_6$ | $(0, 775)\mu$m |
| $\Delta u_7$ | $(-2550, 0)\mu$m |

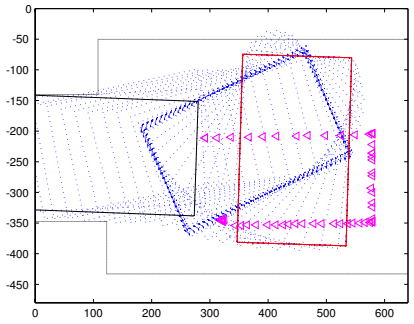

Fig. 6. Data captured from experimental trial using intuitive plan.

the peg are shown in solid lines, while the intermediate steps are pictured with dotted lines. The tip locations are represented with triangles.

Figure 7 shows a detailed comparison between simulation and experimental results for an intuitively designed plan. The discrepancy at time $t = 0$ can easily be explained by the initial peg position error. Subsequent errors are both a result of this initial error as well as inaccuracies of the time-stepping model and its parameters. Note that even with the error in the initial peg position and model inaccuracies, the plan is successful in experimentation and closely matches the simulated data.

## VI. DISCUSSION

This paper addressed the modeling, simulation, and planning of a simple micro-assembly task in which a peg with a characteristic length of 1 mm is reoriented by pushing with a probe and inserted into a hole. We relied on vision to estimate the initial configuration of the system rather than for feedback control. An RRT algorithm was used to produce feasible manipulation plans. While these plans were sometimes successful when carried out experimentally, they were not robust to error associated with the uncertainty in the support friction models or to those associated with the initial positioning of the peg. An intuitive motion plan was generated to increase robustness and executed experimentally to successfully accomplish the task.

While the preliminary results in this paper are promising and illustrate the potential for the use of quasi-static mechanics with models of frictional contact, there are some shortcomings of this study which are also directions of ongoing work.

First, it is necessary to incorporate the uncertainty in surface friction. The three-point support model obtained via system

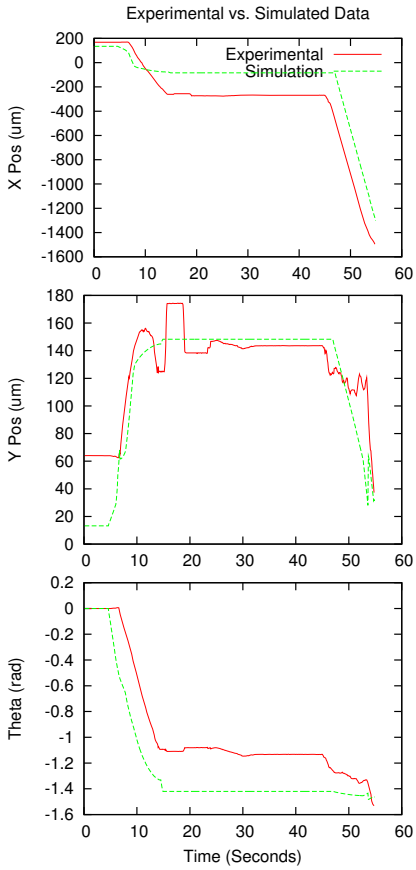


Fig. 7. Plot comparison of insertion plan in simulation and in experimental trial.

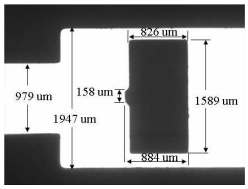


Fig. 8. Photochemically machined parts.

identification provides only a nominal starting point. Our experimental data for unconstrained manipulation allows us to characterize the set of possible three-point supports that might better describe the pressure distribution for the peg.

Second, although our experimental set-up is conducive to measuring contact forces between the probe and the peg, we have not made these measurements for system identification or for ground truth. This is will be addressed in our future work.

Finally, our laser cutting fabrication technique for meso-scale parts was crude as seen from the silhouette in the Figure 4. We have since used a photochemical machining (PCM) process to manufacture a new set of parts. These parts exhibit much better corner and edge features, as seen in Figure 8. Our ability to generate successful manipulation plans for imperfect parts suggests we should be able to do even better with better made components, which we hope to prove with these new parts.

## ACKNOWLEDGMENT

This work was supported by NSF grants DMS01-39747, IIS-0413138 and IIS02-22927.

## REFERENCES

[1] K. Goldberg, "Orientating polygonal parts without sensing," *Algorithmica*, vol. 10, no. 2/3/4, pp. 210–225, August/September/October 1993.

[2] M. Erdmann and M. Mason, "An exploration of sensorless manipulation," *IEEE Journal of Robotics and Automation*, vol. 4, no. 4, August 1998.

[3] M. Moll, K. Goldberg, M. Erdmann, and R. Fearing, "Orienting micro-scale parts with squeeze and roll primitives," *IEEE Int. Conf. on Robotics and Automation, Washington, DC*, May 11-15 2002.

[4] M. Mason, "Manipulator grasping and pushing operations," Ph.D. dissertation, Massachusetts Institute of Technology, 1982.

[5] ——, "Mechanics and planning of manipulator pushing operations," *International Journal of Robotics Research*, vol. 5, no. 3, pp. 53–71, 1986.

[6] M. Peshkin and A. Sanderson, "The motion of a pushed, sliding object, part1: Sliding friction," Robotics Institute, Carnegie Mellon University, Pittsburgh, PA, Tech. Rep. CMU-RI-TR-85-18, September 1985.

[7] P. Song, J. Pang, and V. Kumar, "A semi-implicit time-stepping model for frictional compliant contact problems," *International Journal for Numerical Methods in Engineering*, Accepted for publication 2004.

[8] J. Trinkle, S. Berard, and J. Pang, "A time-stepping scheme for quasistatic multibody systems," *International Symposium of Assembly and Task Planning*, July 2005.

[9] K. Lynch, "The mechanics of fine manipulation by pushing," *IEEE Int. Conf. on Robotics and Automation, Nice, France*, pp. 2269–2276, May 1992.

[10] K. Lynch and M. Mason, "Stable pushing: Mechanics, controllability, and planning," *International Journal of Robotics Research*, vol. 15, no. 6, pp. 553–556, December 1996.

[11] S. Akella and M. T. Mason, "Posing polygonal objects in the plane by pushing," *International Journal of Robotics Research*, vol. 17, no. 1, pp. 70–88, Jan. 1998.

[12] R. Fearing, "Survey of sticking effects for micro parts handling," *IEEE/RSJ Int. Conf. on Intelligent Robotics and Sys.(IROS), Pittsburgh, PA*, vol. 2, pp. 212–217, August 5-9 1995.

[13] K. Boehringer, R.Fearing, and K. Goldberg, *Handbook of Industrial Robotics, 2nd Ed.* John Wiley and Sons, 1999, ch. Microassembly, pp. 1045–1066.

[14] B. Vikramaditya and B. Nelson, "Visually guided microassembly using optical microscopes and active vision techniques," *IEEE Int. Conf. on Robotics and Automation, Albuquerque, New Mexico*, 1997.

[15] P. Song, J. Trinkle, V. Kumar, and J. Pang, "Design of part feeding and assembly processes with dynamics," *IEEE Int. Conf. on Robotics and Automation, New Orleans, LA*, April 2004.

[16] S. LaValle, "Rapidly-exploring random trees: A new tool for path planning," 1998. [Online]. Available: citeseer.ist.psu.edu/lavalle98rapidlyexploring.html

[17] J. Kim, J. M. Esposito, and V. Kumar, "An rrt-based algorithm for testing and validating multi-robot controllers," in *Robotic Science and Systems*, June 2005.

[18] M. Anitescu and F. Potra, "Formulating dynamic multi-rigid-body contact problems with friction as solvable linear complementarity problems," *Nonlinear Dynamics*, vol. 14, no. 3, pp. 231–247, 1997.

[19] D. Stewart and J. Trinkle, "An implicit time-stepping scheme for rigid body dynamics with inelastic collisions and coulomb friction," *International Journal of Numerical Methods in Engineering*, vol. 39, pp. 2673–2691, 1996.